Thesis Title

A subtitle of your thesis

Author name

Thesis submitted for the degree of
Master in Master's Program Name <change at main.tex>
60 credits

Department Name <change at main.tex>
Faculty name <change in duoforside.tex>

UNIVERSITY OF OSLO

Spring 2022

Thesis Title

A subtitle of your thesis

Author name

Thesis Title

http://www.duo.uio.no/

Printed: Reprosentralen, University of Oslo

Abstract

Contents

List of Figures

List of Tables

Preface

Chapter 1

Introduction

some introduction on the importance of discovering new materials and alloying.

High-entropy alloys is a novel class of materials based on alloying multiple components, as opposed to the more traditional binary alloys. This results in an unprecedented opportunity for discovery of new materials with a superior degree of tuning for specific properties and applications. Recent research on high-entropy alloys have resulted in materials with exceedingly strong mechanical properties such as strength, corrosion and temperature resistance, etc **find references**. Meanwhile, the functional properties of high-entropy alloys is vastly unexplored. In this study, we attempt to broaden the knowledge of this field, the precise formulation of this thesis would be an exploration on the possibilities of semiconducting high-entropy alloys.

A key motivation of this thesis is the ability to perform such a broad study of complex materials in light of the advances in material informatics and computational methods. In this project, we will employ Ab initio methods backed by density functional theory on top-of the line supercomputers and software. 20 years ago, at the breaking point of these methods, this study would have been significantly narrower and less detailed firstly, but secondly would have totaled ... amount of CPU hours to complete (**Calculate this number**). In the addition to the development in computational power, is also the progress of modeling materials, specifically we will apply a method called Special Quasi-random Structures (SQS) to model high-entropy alloys or generally computationally complex structures. Together with the open landscape of high-entropy alloys described above, these factors produce a relevant study in the direction of applying modern computational methods to progress the research of a novel material class and indicate promising directions within the field.

In specifics, this thesis revolve around the electrical properties of high-entropy alloys, mainly the band gap as this is the key indicator for a semiconducting material and it's applicability. Semiconductors are the building blocks in many different applications in today's world, ranging from optical and electrical devices, to renewable energy sources such as

solar and thermoelectricity. Given the economic and sustainable factors concerning silicon, in addition to its role in relevant applications such as microelectronics and solar power. Silicon emerges as a natural selection to build our alloys around. Furthermore, the development and research on both high entropy alloys and metal silcides have been heavily centered around 3d transition metals. Keeping in line with the economic and environmental factors, we will continue this direction by focusing on high entropy stabilized sustainable and economic 3d metal silicides **Not happy with this writing**. Throughout the study we will analyze a great number of permutations of 3d silicides, from different initial metal silicides such as $CrSi_2$, $FeSi_2$, $MnSi_{1.75}$, Fe_2Si, each with distinct properties relating to the band gap, crystal structure and metal to silicon ratio. In addition, the permutations include numerous metal distributions and elements within the 3d-group of metals. Examples are Co, Cr, Fe, Mn, and Ni.

Given a background in high-entropy alloys, one could ask if this study is truly sensible. In the later sections we will cover the details of this field, and it quickly become clear that the materials investigated in this study does not fall under the precise definition of high-entropy alloys, nor do we intend to explore the properties and factors relating to high-entropy stabilized alloys such as the configurational entropy, phase stability and finite temperature studies. However this study is motivated from the discovery of these materials and promising properties, and venture into a more hypothetical space of materials, enabled by the computational methods available to study the potential properties of such materials. On the other hand, very recent studies **Mari, and other HEA silicide study** have experimentally produced high-entropy disilicides, thus in some way justifying the direction of this project.

We begin this project by reviewing key concepts of solid-state physics for readers lacking a background in materials science, and an introduction to the base 3d silicides of the experimental work. Later follows a theoretic walk-through of the relevant concepts of this thesis, these topics include high-entropy alloys, special quasi-random structures, and density functional theory. Next we shine light on the implementation of DFT in this project, and other computational details required to reproduce the results in this thesis, such as the use of the Vienna Ab Initio Simulation Package (VASP) and implementation of SQS. Finally we present the results of our study, these include the band gap and electronic properties of various structures and the success and challenges of the computational methods applied throughout the study.

Part I

Theory

Chapter 2

Background

References: "Introduction to Solid-State physics", "Understanding solids", "Sold-state electronic devices", databases

2.1 Overview of sold-state physics

- Crystal structure
- Reciprocal lattice + Brilluin zone
- Chemical bonding + orbitals + energy bands
- Band gap + DOS ++

2.2 3d Silicides

In this project, we will build high-entropy silicides based on several promising 3d silicides, in terms of particularly the band gap. The silicides are $CrSi_2$, $MnSi_{1.75}$, $FeSi_2$ and Fe_2Si. A summary of their most relevant properties for this project is listed in table .., and their corresponding crystal structure is displayed in figure ..

More information on these here...

Chapter 3

High-Entropy alloys

To begin this project, we give a brief description of high-entropy alloys (HEA). We introduce the basics and definitions, as well some more advanced topics relating to the functional properties of HEA's. This section will be largely based on the fantastic description of HEA's in "High-Entropy Alloys - Fundamentals and Application" and the references therein, it's an excellent read. This section is particularly based on chapters 1,2,3, and 7 [29], [32], [30], [31]

3.1 Fundamentals

High-Entropy Alloys are a quickly emerging field in materials science due to the infinitely many possibilities and the unique properties. From the original discovery by Jin in 2004, as of 2015 there have been over 1000 published journal articles on high-entropy alloys. In its simplicity, a high-entropy alloy can be compared to a smoothie. By combining an assortment of fresh fruit and vegetables one can produce unique combinations of flavors and nutritional values based on both the properties of the distinct items, and their interplay in the mixture. In materials science, this exact procedure can be applied to generate a large range of materials with tunable properties depending on the intended application. In the topic of HEA's, this can be increased strength or ductility, corrosive resistance or lowered thermal conductivity, all of which have been observed in actual high-entropy alloys. Moving on from the rather banal fruit analogy, a high-entropy alloy typically falls under the two conditions.

1. The material consist of at least 5 distinct elements, where each element contribute between 5-35% of the composition
2. The total configurational entropy is greater than 1.5R, where R is the gas constant.

The latter is an especial case for high-entropy alloys. The ideal configurational entropy of random N-component solid-solution is given in eq 3.1

$$\Delta S_{\text{config}} = -R \sum_{i=1}^{N} X_i \ln X_i, \tag{3.1}$$

it's clear that ΔS_{config} increase with a higher number of constituents in the mix. For instance, the ideal configurational entropy of a binary alloy is $0.69R$, while a 5-component alloy is $1.61R$. If we neglect other factors that influence the formation of solid solutions (will be covered later), from Gibbs free energy in eq 3.2

$$\Delta G_{\text{mix}} = \Delta H_{\text{mix}} - T\Delta S_{\text{mix}}, \tag{3.2}$$

the two primary factors in formation of solid solution is the mixing enthalpy, which is the driving force to form compounds, and the mixing entropy which is the driving force to form random solid solutions. At elevated temperatures especially, the energy associated to the entropy of the system becomes comparative to the mixing enthalpy and can impact the overall equation. In summary, the overall concept of high-entropy alloys is that through alloying a greater number of elements, the gain in configurational entropy of the system prohibit the formation of intermetallic compounds in favor of a random solid solution. The random term simply relate to the various components occupying lattice positions based on probability. In fact, a narrower definition of high-entropy alloys would be structures with a single-phase disordered solid solution. The two "definitions" given previously can be considered as guidelines for the latter.

All though the mixing entropy mentioned above plays a central role in the formation, there are other factors to consider, and some that may oppose the formation of a single disordered phase. One of these is the atomic size effect which is related to the differences in atomic size, between the various elements in the alloy, this quantity is denoted δ. Y. Zhang et al. in 2008 illustrated the relationship between ΔH_{mix} and δ. When δ is very small, ie similar atomic sizes. The elements have an equal probability to occupy lattice sites to form solid solutions, but the mixing enthalpy is not negative enough to promote formation of solid solution. Increasing δ does result in greater ΔH_{mix}, but leads to a higher degree of ordering. **Include figure?**To summarize the illustration, the formation of solid solution high-entropy alloys occur in a narrow range of δ value that satisfy both the enthalpy of mixing and the disordered state. Recently, Yang and Zhang proposed the parameter Ω to evaluate the stability of high-entropy alloys. The quantity is a product of the melting temperature T_m, mixing entropy and mixing enthalpy in the following manner

$$\Omega = \frac{T_{\text{m}}\delta S_{\text{mix}}}{|\Delta H_{\text{mix}}|}. \tag{3.3}$$

. They managed to obtain a qualitative condition for formation of the single disordered solid solution at $\Omega \geq 1.1$ and $\delta \leq 6.6\%$. While compounds such as intermetallics form for greater values of δ and lesser values of Ω. Similarly, replacing the atomic size effect constant for the number of elements result in an equivalent condition. The results are summarized in figure 3.1

An important quantity in terms of characterizing high-entropy alloys is the total number of electrons VEC. The valence electron concentration of

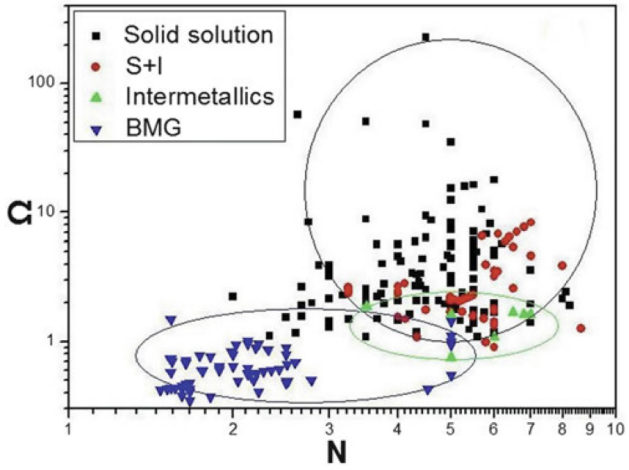

(a) HEA formation based on Ω and δ

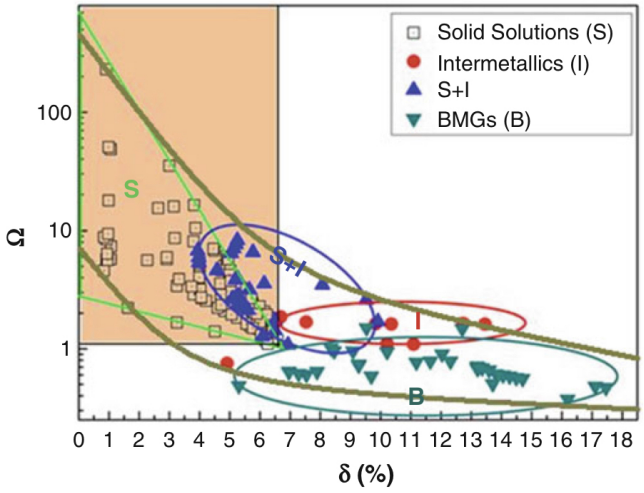

(b) HEA formation based on Ω and N

Figure 3.1: Formation of HEA based on δ and N. Figures adopted from [32]

a material is strongly related to the crystal structure of the material. For example, Co_3V, originally a hexagonal structure can be transformed into a tetragonal or cubic structure by either increasing the VEC from alloying with Ni, or reduction with Fe respectfully. Derived from the work of Guo et al. on the phase stability of a $Al_xCrCuFeNi_2$ HEA, the VEC can be directly related to the crystal structure of high-entropy alloys. A lower VEC stabilize the BCC phase, while higher values stabilize FCC. In between is a mixture of the two. Specifically values greater than 8.0 stabilize FCC, and values bellow 6.87 favor BCC. However, these boundaries is not rigid when including elements outside of transition metals, exceptions has also been found for high-entropy alloys containing Mn. All though a heavy majority of reported high-entropy alloys that form solid solutions have been found to adopt simple cubic structures such as FCC and BCC. Recent studies have observed HEA's in orthorombic structures like $Ti_{35}Zr_{27.5}Hf_{27.5}Ta_5Nb_5$ and hcp structures, for example $CoFeNiTi$.

3.2 Core effects and properties of high-entropy alloys

Next, we will summarize the discussion above into four core elements that distinctly describe high-entropy alloys and their implications on the functional properties. The first of these is the "high-entropy effect", as the name suggests this is related to the increased configurational entropy from the amount of elements, that can inhibit the formation of strongly ordered structures. The second effect is the "severe lattice distortion effect", that originates from the fact that every element in a high-entropy structure is surrounded by non-homogeneous elements, thus leading to severe lattice strain and stress. The overall lattice distortion is additionally attributed to the differences in atomic size, bonding energies and crystal structure tendencies between the components. Therefore the total lattice distortion observed in HEA's are significantly greater than that of conventional alloys. This effect mostly affect the strength and conductivity of the material, such that a higher degree of distortion yields greater strength and greatly reduces the electronic and thermal conductivity due to increased electron and phonon scattering. An upside to this is that the scattering and following properties become less temperature dependent given that it originates from the lattice rather than thermal vibrations.

The two remaining effects, "sluggish diffusion" and "cocktail effect" can be summarized swiftly. The first is a direct consequence of the multi-component layout of high-entropy alloys that result in slowed diffusion and phase transformation because of the number of different elements that is demanded in the process. The most notable product from this effect is an increased creep resistance. Lastly we have the cocktail effect, which is identical to the smoothie analogy mentioned previously, in that the resultant characteristics is a combination of both the elements and their interaction. This is possible the most promising concept behind high-entropy alloys, which fuels researchers with ambition to discover highly optimized materials by meticulously combining and predicting

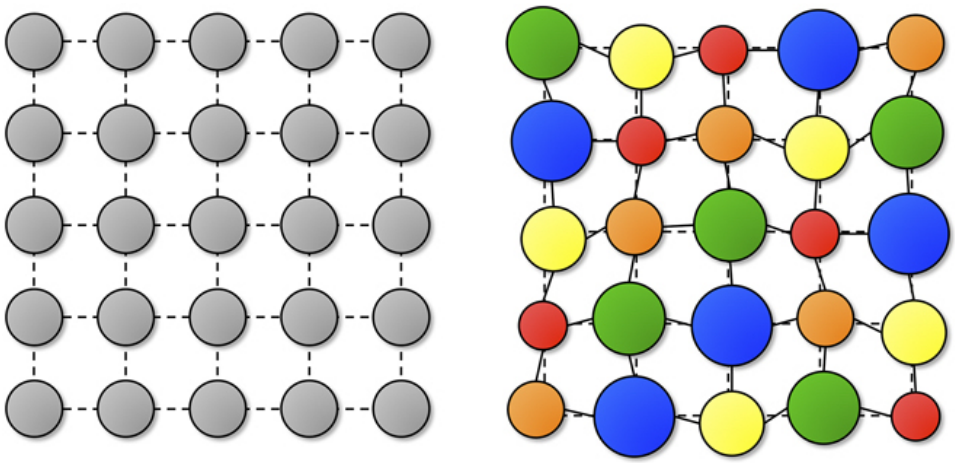

Figure 3.2: A schematic illustration of lattice distortion in high-entropy alloys. Figure from [13]

properties from different elements. Examples of this can be the refractory HEA's developed by "Air Force Research Laboratory" severely exceeding the melting points and strength of previous Ni or Co-based superalloys by alloying specifically refractory elements such as Mo. Nb and W. Another example is the research conducted by Zhang et al. on the high-entropy system $FeCoNi(AlSi_{0-0.8}$ in the intent of unveiling the optimal combination of magnetic, electric and mechanical properties, resulting in an excellent soft magnet.

In the discussion above, we have covered the four core effects that make up high-entropy alloys and their relation to the mechanical and functional properties. Of the core effects, especially the lattice distortion and cocktail effect relate to the functional properties. The initial study on the functional properties on high-entropy alloys was conducted on the H-x alloy, referring to the system $Al_xCoCrFeNi$ with $0 \leq x \leq 2$. It was found that the electrical resistivity was higher than that of conventional alloys, and that the conductivity generally decreased with increasing amounts of Al, additionally noteworthy low carrier mobility. Similar findings have also been made for the high-entropy alloy $FeCoNi(AlSi)_x$.

Write a small part on magnetic and relate to the cocktail effect, then very briefly conclude by mentioning findings of superconductivity, corrosion resistance, hydrogen storage and other properties/applications.

Chapter 4

Special quasi-random Structures

The structure of high-entropy alloys in which the alloying elements occupy lattice sites by a random probability pose a problem on the numerical methods used for modeling. DFT in particular rely heavily on the periodicity in crystalline solids, as we will discover later. Some of the popular current tools for overcoming this problem of modeling a chemically disordered compound in the framework of density functional theory, are the virtual crystal approximation (VCA), Coherent Potential approximation (CPA), special quasi-random structure (SQS), and hybrid monte-carlo/molecular dynamics. (MC/MD). A brief review of the different models is given in for example [23]. In this project we will exclusively use SQS to model random alloys, in large part from it's easy to use implementation and interpretation in VASP compared to the other options. However, SQS does offer certain benefits that will become clear throughout the following sections.

4.1 The fundamentals of SQS

Before the arrival of SQS and CPA methods, the common approach of modeling random alloys was to distribute the numerous elements randomly over the lattice sites. This was a costly operation, which either involved averaging a great number of possible configurations, or infeasible large supercells considering the computational efforts required. In the original paper on SQS published in 1990 [28], it was proposed a selective occupation strategy to design special periodic quasi-random structures that exceed previous methods in accuracy and cost. The key concept was to create a periodic unit cell of the various components in a finite N lattice site single configuration such that the structure most closely resemble the configuration average of an infinite perfect random alloy. In an attempt to work withing the 50 lattice sites boundary of ab initio methods at that time. The working theory was that if one can resemble an infinite perfect random alloy by a periodic finite N cell, also the electronic properties would be similar between the two. The solution to this model was that for

each N, ie lattice site, to minimize the difference of structural correlation function between the approximated cell and the perfect random alloy. There are obviously errors involved with approximating a random alloy by a periodic cell, but by the hierarchical relation to the properties of the material, interactions between distant sites only offer a negligible small contribution to the total energy of the system. Thus the aim of the SQS method is focused around optimizing the correlations within the first few shells of a given site. To follow is a review of the mathematical description of special quasi-random structures.

4.2 Mathematical formulation

We begin this section by giving a brief review of topics such as cluster expansions, statistics and superposition of periodic structures. A broader description of these topics can be found in the original article, or elsewhere in the literature. On a side note regarding the following mathematical derivation, the original concept was devolved in mind of an random binary alloy, but the theory have late successfully been extended to multi-component alloys and other special cases.

The different possible atomic arrangements are denoted as "configurations" σ. The various physical properties of a given configuration is $E(\sigma)$, and $< E >$ is the ensemble average over all configurations σ. In practice, this quantity is unfeasible in terms of computational cost, seeing as the average require calculations and relaxations of all possible configurations, for a binary alloy this is 2^N for a fixed N number of lattice sites. A solution to this is to use the theory of cluster expansions and discretize each configuration into "figures" f. A figure in the lattice is defined in terms of the number of atoms it include k, distance in terms of neighbors m, and position in the lattice l. Further we assign spin values for each lattice site i in the figure to denote which element it holds (+1,-1 for a binary alloy). By defining the spin product of spin variables in a figure at lattice position l as $\Pi_f(l, \sigma)$, we can write the average of all locations in the lattice of a given figure f as

$$\mathbf{\Pi}_f(\sigma) = \frac{1}{ND_f} \sum_l \Pi_f(l, \sigma) \tag{4.1}$$

where D_f is the number of equivalent figures f per site. The brilliance of this notation is that we now can express the physical property $E(\sigma)$ in terms of the individual contributions ϵ_f of a figure f.

$$E(\sigma) = \sum_{f,l} \Pi_f(l, \sigma) \epsilon_f(l) \tag{4.2}$$

The quantity ϵ_f is called the "effective cluster property" and is defined as (for a random binary alloy $A_{1-x}B_x$)

$$\epsilon_f(l) = 2^{-N} \sum_{\sigma}^{2^N} \Pi_f(l, \sigma) E(\sigma) \tag{4.3}$$

Inserting the equation for $\mathbf{\Pi}_f$ into that of $E(\sigma)$ we can describe the the previous cluster expansion of $E(\sigma)$ as

$$E = N \sum_f D_f < \mathbf{\Pi_f} > \epsilon_f \tag{4.4}$$

And obtain a simplified expression for $< E(\sigma >)$ in eq 1? Thus we have successfully managed to reduce the expensive task of sampling all $E(\sigma)$ into calculating the effective cluster properties and summing over all types of figures. Remembering that $E(\sigma)$ can relate to many physical properties, the most common and applied case is that $E(\sigma)$ is the total energy, while ϵ_f is many body interaction energies. The cluster expansion above converge rather quickly with increasing number of figures, an effective method is thus to select a set of configurations to evaluate the effective cluster properties. Don't know how to write this, but the next step is to select a finite largest figure denoted F, and "specialize" the cluster expansion to a set of N_s periodic structures σ =s to obtain the two expressions for $E(s)$ and ϵ_f using matrix inversion to obtain the result for ϵ_f

$$E(s) = N \sum_f^F D_f \mathbf{\Pi}_f(s) \epsilon_f \tag{4.5}$$

$$\epsilon_f = \frac{1}{ND} \sum_s^{N_s} [\mathbf{\Pi}_f(s)] - 1E(s) \tag{4.6}$$

Assuming now that the sum of figures F and N_s periodic structures are well converged, $E(\sigma)$ can be rewritten as a superposition of $E(s)$

$$E(\sigma) = \sum_s^{N_s} \xi_s(\sigma) E(s) \tag{4.7}$$

$$\xi_s(\sigma) = \sum_f^F [\mathbf{\Pi}_f(s)]^{-1} \mathbf{\Pi}_f(\sigma) \tag{4.8}$$

where ξ is the weights. Thus we have effectively reduced the problem to a convergence problem of the number of figures F and structures N_s. This can be easily solved given that we are dealing with periodic crystal structures s that can employ the general applications of ordered structures from ab initio methods, and increasing F until the truncation error falls bellow a desired threshold. However, this approach requires that the variance of the observable property is much lower than the sample mean, otherwise one would have to employ a much bigger sample size to reach statistical convergence. Don't how to write this part nicely, but: Because of the different relationship between various physical properties and the correlation functions, one observe different convergence depending on the meaning of E. The idea behind SQS was therefore to design single special structures with correlation functions $\mathbf{\Pi}_f(s)$ that most accurately match those of the ensemble average of a random alloy $< \mathbf{\Pi}_f >_R$.

The correlation functions of an perfect random infinite alloy, denoted as R is defined bellow

$$\mathbf{\Pi}_{k,m}(R) =< \mathbf{\Pi}_{k,m} >_R = (2x - 1)^l \tag{4.9}$$

with k, m defined as before and x being the composition ratio of the alloy. In the case of an eqvimolar alloy ($x = \frac{1}{2}$), the functions equal 0 for all k except $< \mathbf{\Pi}_{0,1} >_R = 1$. If we now randomly assign either atom A or B to every lattice site, for a sufficiently large value of N, the goal is then to create a single configuration that best match the random alloy. Keeping with the $x = \frac{1}{2}$ case, the problem is now that even though the average correlation functions of a large set of these structures approaches zero, like for the random alloy. The variance of the average is nonzero meaning that a selected structure of the sample is prone to contain errors. The extent of these errors can be evaluated from the standard deviations

$$\nu_{k,m}(N) = | < \mathbf{\Pi}^2_{k,m} > |^{\frac{1}{2}} = (D_{k,m}N)^{-\frac{1}{2}} \tag{4.10}$$

Given the computational aspects, it's obvious that economical structures with small N are prone to large errors. In fact, in some cases these errors can result in correlation functions centering around 1, as opposed to 0 for a perfect random alloy.

I don't know how to write the prelude to this part! (see section IIIA in [28]). The degree to which a structure s fails to reproduce the property E of the ensemble-averaged property of the random alloy can be described by a hierarchy of figures, see eq .. bellow

$$< E > -E(s) = \sum_{k,m}^{\prime} D_{k,m}[(2x-1)^k - \mathbf{\Pi}_{k,m}(s)]\epsilon_{k,m} \tag{4.11}$$

, the prime is meant symbolize the absence of the value $0, 1$ for k, m. The contribution from the figure property ϵ reduces for larger figures. In general, for disordered systems, the physical property "E" at a given point R falls of exponentially as $|R - R'|/L$, where L is a characteristic length scale relating to the specific property. Using this, the approach of SQS is to specify a set of correlation functions that hierarchically mimic the correlation functions of the random alloy. Meaning that it prioritize the nearest neighbor interactions. With the set of functions decided on, the objective it finally to locate the structures that correspond to the selected structures.

With this approach, [28] managed by mimicking the correlation functions exact for the first two shells, to reduce the computational measures of an accurate models. In this exact study they matched the results of an $N \to \infty$ by an $N = 8$ SQS. In the final section of this chapter, we will take a look at the recent advances in the SQS method and application to high-entropy alloys.

4.3 Application of SQS to high-entropy alloys - Add figure

The success of the SQS-approach is related to to the fact that we create simple periodic structures that allow for standard DFT based methods to calculate properties such as the total energy, charge density and

electronic band structure [12], [26]. However, the application to high-entropy alloys have been limited prior to the last couple of years on the grounds of computational demands involved in modeling disordered multi-component systems and the very recent emergence of the field in general. Mainly the last few years have we seen studies of high-entropy alloys based on special quasi-random structures [25], [27], [18], [20].

From the pioneering work of M.C Gao et al. [5], whom in 2016 presented a comprehensive review high-entropy alloys modeling with SQS based on ab initio simulations in the framework of DFT and VASP, majorly $CoCrFeNi$ and $CoCrFeMnNi$. It's apparent that the physical accuracy of SQS-models and their corresponding properties are very sensitive to the size of the supercell, or more generally the total number of atoms. Typically, cells with more than 64 atoms, often 125 or even 250 atoms were required to match experimental findings and results from other modeling techniques such as MC/MD and CPA. Examples are the predicted ground-state structure and pair distribution functions (PDFs). The key takeaway from the work of M.C Gao et al. can then be that in order for special quasi-random structures to accurately model the disordered structure of high-entropy alloys, a large number of atoms is required. Another point to this is that in addition to chemical disorder, HEAs possess a disordered magnetic structure. Considering the computational aspects, this means the optimal magnetic configuration is difficult to locate in high-entropy alloys and may contribute to the incorrect predictions in certain cases.

How to I write this final paragraph of why SQS is used at HEAs today? mcSQS? Something on in very recent time, computational resources have increased and the generation of SQS have improved by the mc-SQS approach? This allows for a reduction in cell size and computation time, all though the convergence of SQSs and magnetic configuration remain troublesome in some cases. Maybe mention that the implementation of the TDEP package drastically improve the computational cost.

Chapter 5

Density-Functional Theory

References for theory: fys-mena4111 lecture notes and book

5.1 Review of Quantum Mechanics

5.1.1 The Shrödinger equation

The Schrödinger equation composed of the wavefunction $\Psi(\vec{r},t)$ and Hamiltonian $\hat{H}(\vec{r},t)$ where $\vec{r}$ and t is the spatial position and time respectfully.

$$i\hbar\frac{\partial}{\partial t}\Psi(\vec{r},t) = \hat{H}(\vec{r},t)\Psi(\vec{r},t) \tag{5.1}$$

The time-independent shr0̈dinger equation for the eigenvalues E_k of the k-th eigenvalue $\psi_k(\vec{r}$

$$\hat{H}\psi_k(\vec{r}) = E_k\psi_k(\vec{r}) \tag{5.2}$$

Extending to a system comprised of multiple particles, we have the many-particle Shrödinger equation, involving the many-body Hamiltonian. This quantity is composed of the kinetic energy of N_e electrons T_e, the interaction energy between electrons U_{ee}, the kinetic energy of N_n nuclei, the coulomb interaction between nuclei U_{nn}, and finally the attractive interaction between nuclei and electrons U_{en}. In the equation bellow for the may-body equation, we use the following symbols and notation: m_e = electron mass, m_n = nuclei mass, ϵ_0 = permittivity in vacuum, q = particle charge, α = nuclei number, Z_a = atom number of nuclei α, r = position of electron, R = position of nuclei.

$$\hat{H} = T_e + T_n + U_{ee} + U_{nn} + U_{en} \tag{5.3}$$

$$\begin{aligned} &= -\sum_{j=1}^{N_e}\frac{\hbar^2\nabla_j}{2m_e} - \sum_{\alpha=1}^{N_n}\frac{\hbar^2\nabla_\alpha}{2m_n} + \frac{1}{4\pi\epsilon_0}\sum_{j=1}^{N_e}\sum_{j'<j}\frac{q^2}{|r_j - r_{j'}|} \\ &+ \frac{1}{4\pi\epsilon_0}\sum_{\alpha=1}^{N_n}\sum_{\alpha'<\alpha}\frac{q^2 Z_\alpha Z_{\alpha'}}{R_\alpha - R_{\alpha'}} - \frac{1}{4\pi\epsilon_0}\sum_{j=1}^{N_e}\sum_{\alpha=1}^{N_n}\frac{q^2 Z_\alpha}{|r_j - R_\alpha|} \end{aligned} \tag{5.4}$$

5.1.2 Simplifications and approximations to solve the many-electron Shrödinger equation

Born-Oppenheimer

Challenges with solving many-particle Shrödinger equation is i) computationally expensive, ii) need to know how Ψ depends on single particle wavefunctions ψ_k. To solve this complex problem, we need approximations. Particularly Born-Oppenheimer and Harte-Fock approximations. The first makes the cleaver and reasonable assumption that since the electron mass is negligibly small in comparison to that of a nuclei, we can treat the nuclei as point charges, enabling us to divide the eigenfunction into a separate electronic and nuclear part, ie

$$\Psi_k^{en}(\vec{r}, \vec{R}) \approx \Psi_k(\vec{r}, \vec{R})\Theta_k(\vec{R}) \tag{5.5}$$

where we have written the complete wavefunction in terms of an electronic part $\Psi_k(\vec{r}, \vec{R})$ and nuclear part $\Theta_k(\vec{R})$. The dependencies come from the fact that electrons can respond instantaneously to new positions of the nuclei, therefore the $\vec{R}$ dependence. Writing this in terms of the Hamiltonian we get

$$\left(T_e + U_{ee} + U_{en}\right)\Psi_k(\vec{r}, \vec{R}) = E_k(\vec{R})\Psi_k(\vec{r}, \vec{R}) \tag{5.6}$$

$$\Big(T_n + U_{nn} + E_k(\vec{R})\Big)\,\Theta(\vec{R}) = E_k^{en}(\vec{R})\Theta_k(\vec{r}, \vec{R}). \tag{5.7}$$

The two sections are interrelated through the electronic energy eigenvalue $E_k(\vec{R})$. Furthermore, the left hand side of the nuclear part can be simplified to $U_{nn} + E_k(\vec{R})$, assuming that the kinetic energy of point charges is zero. This simplified expression for the nuclear left hand side is called for the potential energy surface (EPS).

Hartree-Fock

The next step in line is to find a wavefunction that can describe all electrons in a system. This was originally done by Hartree, which assumed that electrons can be described independently and suggested the ansatz for a two-electron wavefunction

$$\Psi_k(\vec{r_1}, \vec{r_2}) = A \cdot \psi_1(\vec{r_1})\psi_2(\vec{r_2}), \tag{5.8}$$

where A is the normalization constant. However this approximation does not account for the fact that electrons are indistinguishable and hence does not obey the Pauli exclusion principle for ferminons. This was overcome with the Hartree-Fock approximation that implement an anti-symmetric wavefunction. The full expression is given bellow

$$\Psi_k(\vec{r_1}, \vec{r_2}) = \frac{1}{\sqrt{2}}\Big(\psi_1(\vec{r_1})\psi_2(\vec{r_2}) - \psi_1(\vec{r_2})\psi_2(\vec{r_1})\Big) \tag{5.9}$$

The Hartree-Fock (HF) approximation makes the electrons distinguishable and hence obey the Pauli exclusion principle, this means that the exchange energy is accounted for. On the other side, HF is not a complete description as it fails to model the electron correlations.

The Variational principle

In materials science, the overarching concern is the ground-state properties of a system. This can be found efficiently and easy by whats known as the variational principle. This states that the energy of any trial wavefunction will always be higher than the ground-state energy E_0, ie

$$E_0 = \langle \psi_0 | H | \psi_0 \rangle \leq \langle \psi | H | \psi \rangle = E \tag{5.10}$$

This enable us to find the ground state energy and corresponding wavefunction by a minimization technique. Next, we will present the basics of the density functional theory for how these equations can be solved numerically and efficiently in order to study real materials and systems.

5.2 Fundamentals of Density-Functional Theory

The density functional theory was developed by Hohenberg and Kohn in 1964 and revolved around the fact that the ground-state density can be expressed in terms of the ground-state wavefunction. We have

$$n_0(r) = |\Psi_0(r)|, \tag{5.11}$$

furthermore the theorem states that all ground-state physical properties can be found as unique functionals of the ground-state density. The biggest upside of this, is that instead of trying to solve the many-body Shrödinger equation to obtain the ground-state wavefunction, we have reduced the computational complexity from $3N_e$ to 3. Thus, the Hohenberg and Kohn density functional theory makes for a promising and effective method to obtain the ground-state properties of a system, given that the exact electron density functional is known. However, this is still 60 years later unknown.

The density functional theory build on two specific theories, called the Hohenberg-Kohn theorems. They are:

1. For any system of interacting particles in an external potential V_{ext}, the density is uniquely determined.

2. There exists a variational principle for the energy density functional such that, if n is not the electron density of the ground-state, them $E[n_0] < E[n]$.

The proof behind both theorems can be found in appendix .. A direct result of the second theorem is the energy can be described as a function of the density

$$E[n] = T[n] + U_{ee}[n] + U_{en}[n], \tag{5.12}$$

where the first two terms $T[n]$ and $U_{ee}[n]$ make up the Hohenberg-Kohn functional.

We know move on to the Kohn-Sham equations, in which Kohn and Sham expressed the exact ground-state density from Hartree type wavefunctions.

$$\Psi(\vec{r}_1, \vec{r}_2, .., \vec{r}N_e) = \psi_1^{KS}(\vec{r}_1)\psi_2^{KS}(\vec{r}_2)...\psi_{N_e}^{KS}(\vec{r}_{N_e}) \tag{5.13}$$

In which, ψ_j^{KS} are auxiliary independent single-particle wavefunctions. We know modify the equation for total energy as a function of density defined by the second theorem, to include the single auxiliary wavefunctions and their corresponding kinetic energy and interaction energy. We get:

$$E[n] = T_s[n] + U_s[n] + U_{en}[n] + (T[n] - T_s[n]) + (U_{ee}[n] - U_s[n]). \tag{5.14}$$

with the s subscript denoting the single particle wavefunctions. The latter two terms are known as the exchange-correlation energy E_{xc}

$$E_{xc}[n] = \Delta T + \Delta U \tag{5.15}$$

This term is responsible for the many-electron interaction. The complete total energy functional can now be expressed as

$$\begin{aligned} E[n] = &\overbrace{\sum_j \int \psi_j^{KS*} \frac{-\hbar^2\nabla^2}{2m} \psi_j^{KS} d\vec{r}}^{T_s[n]} + \overbrace{\frac{1}{2}\frac{1}{4\pi\epsilon_0}\int\int q^2 \frac{n(\vec{r})n(\vec{r}')}{|\vec{r}-\vec{r}'|} d\vec{r}\vec{r}'}^{U_s[n]} \\ &+ \underbrace{\int V_{en}(\vec{r}n(\vec{r})d\vec{r}}_{U_e n[n]} + \underbrace{(T[n] - T_s[n]) + (U_{ee}[n] - U_s[n])}_{E_{xc}[n]} \end{aligned} \tag{5.16}$$

Finally we write the complete expression for the Kohn-Sham single-electron equations given an exact exchange-correlation energy and utilizing the variational principle described previously

$$\left\{ -\frac{\hbar^2}{2m_e}\nabla_s^2 + v_H(\vec{r}) + V_{en}(\vec{r}) + V_{xc}(\vec{r}\right\} \psi_s^{KS}(\vec{r}) = \epsilon_s^{KS}(\vec{r})\psi_s^{KS}(\vec{r}), \tag{5.17}$$

Define V_H, and V_{xc} and mention that the former include self interaction that can be accounted for in XC functional. Finally, the total energy of the many-electron system is defined as

$$E[n] = \sum_j \epsilon_j^{KS} - \frac{1}{2}\frac{1}{4\pi\epsilon_0}\int\int q^2 \frac{n(\vec{r})n(\vec{r}')}{|\vec{r}-\vec{r}'|} d\vec{r}d\vec{r}' + E_{xc}[n] - \int V_{xc}(\vec{r})n(\vec{r})d\vec{r}. \tag{5.18}$$

This is the fundamental working principle of the density functional theory and Kohn-Sham equations.

5.3 Limitations of DFT

- Local minima method

- Not exact V_{xc}, means we must compromise between accuracy and cost, and choose between the different methods for specific application. There is no one best overall method that is superior for all purposes.
- kohn-sham eigenfunctions are not the exact eigenfunctions.
- DFT in its original formulation is only valid for the ground state. Thus excited state application of DFT, all though very possible have a lesser theoretical footing.
- The band-gap calculation is also complicated by the self-interaction error which arises in the occupied states in standard DFT, and in the unoccupied states in Hartree-Fock. If you consider the "true" band-structure, then semi-local DFT has a spurious self-interaction in the occupied states, which over-delocalises them and forces them up in energy, thus reducing the band-gap; Hartree-Fock has the same problem but for the *unoccupied* states, so they are over-delocalised and forced up in energy, which increases the band-gap. [7]
- References on the band gap with DFT based methods [17], [16]

Part II

Methodology and Implementation

Chapter 6

Practical application of DFT

In this section we will present the practical application and implementation of density functional theory in the study of materials science.

6.1 The Exchange-Correlation functional

[3] is a good reference for the results regarding the band gap of different solids for a number of functionals

From the former section, we know that the only peace of information we require to perform DFT plane-wave calculations are that of the exchange-correlation energy $E_{\text{xc}}[n]$. Only for a homogeneous electron gas (HEG) is the exact exchange-correlation energy known. The HEG is of limited use in practical application considering that the variation in the electronic concentration is responsible for a wide range of properties. However, the local density approximation (LDA) have found large sucsess from building on the HEG. In the LDA, $E_{\text{xc}}[n]$ is approximated by an electron in an homogeneous electron gas of density $n(\boldsymbol{r})$.

$$E_{\text{xc}}^{\text{LDA}}[n(\boldsymbol{r})] = \int n(\boldsymbol{r})\epsilon_{\text{xc}}[n(\boldsymbol{r})]d\boldsymbol{r}. \tag{6.1}$$

The success of this approach is most dominant in systems with slowly varying charge density, ie bulk materials. A notable downside of LDA is the degree of self-interaction, by only including the local environment, which lead to artificial contributions to the electron density. A significant upside of this method is the low computational cost. **More on LDA?**

A natural succession to the local density approximation is the family of generalized gradient approximation (GGA).

$$E_{\text{xc}}^{\text{GGA}}[n(\boldsymbol{r})] = \int f(n(\boldsymbol{r}), \nabla n(\boldsymbol{r}))d\boldsymbol{r}. \tag{6.2}$$

GGA improves on LDA by additonly considering the gradient of the electron concentration. There currently exists many approaches for how to construct the function f to include the gradient, the two most common are Perdew-Wang 91 (PW91) [15] and Perdew-Burke-Ernzerhof (PBE) [14].

Further, we can extended this idea to include the laplacian ∇^2 of the density. This range of methods is called meta-GGA, popular implementations include *Modified Becke and Johnson* (MBJ) [24] and *Strongly Constrained Appropriately Normed* (SCAN) [21]. **Write a brief discussion of these, see for example [22]**.

Very precise calculations can be obtained from combining LDA/GGA with the exact Hartree-Fock exchange energy. This method was proposed by Becke as hybrid functionals, since the functional is a hybrid between the two. **Insert eq for hybrid functionals?** This method is superior in describing localized states, but comes at a significant larger computational cost. In order to reduce this cost, Heyd al et. split the Hartree-Fock exchange into short-range and long-range parts, in which calculations can adapt exact Hartree-Fock exchange for short-range (SL) and non-exact for long-range (LR). By introducing the parameter ω to adjust the order parameter of the method, we can express this method, called HSE (Heyd-Scuseria-Ernzerhof) [8] as

$$E_{xc}^{HSE} = \alpha E_x^{HF,SR}(\omega) + (1-\alpha)E_x^{PBE,SR}(\omega) + E_x^{PBE,LR}(\omega) + E_c^{PBE} \tag{6.3}$$

Explain what the different notations mean Write more/better on hybrid functionals and HSE06, see references [6], [9]. [11] and write a summary of the different approximations

Over the last 50 years, over 500 different approximations have come to fruition, but mainly PBE GGA, and HSE06 have found wide-spread application and usage [3].

6.2 Fundamental aspects of practical DFT calculations

Needs work, see mainly DFT book ch 3 With the exchange-correlation functionals presented above, we now have everything in order to perform DFT calculations. To begin solving eq .., we need the single-electron wave-function, for a free electron this is a plane wave $\psi_k = Ae^{i\boldsymbol{k}\boldsymbol{r}}$. In a solid however, there exist a nonzero periodic potential $V(\boldsymbol{r}) = V(\boldsymbol{r}+\boldsymbol{R})$, the solution to the Shrödinger equation is given by Bloch's theorem wich states that the solution takes the form

$$\psi_{\boldsymbol{k}}(\boldsymbol{r}) = u_{\boldsymbol{k}}(\boldsymbol{r})e^{i\boldsymbol{k}\boldsymbol{r}}, \tag{6.4}$$

where $u_{\boldsymbol{k}}(\boldsymbol{r})$ is a bloch wave with the periodicity of the supercell, and $\boldsymbol{k}$ is the wavevector. Similar to eq(above), k-space, or reciprocal space is useful to solve the numerous mathematical problems posed by DFT. For instance a great deal of DFT calculations revolve around solving the integral

$$g = \frac{V_{\text{cell}}}{(2\pi)^3}\int_{\text{BZ}} g(\boldsymbol{k})d\boldsymbol{k}, \tag{6.5}$$

with BZ denoting that the integral be evaluated for all $\boldsymbol{k}$ in the Brillouin zone. This integral can be approximated by evaluating the integral at a set of discrete points and summing over the points with appropriatly assigined

weigts. A larger set of points leads to more exact approximations. This method is called Legendre quadrature. The method for selceting these points in reciprocal space was devolped by Monkhorst and Pack in 1976, and simply put requieres a amount of kpoints in each direction in reciprocal space, in the form $NxNxN$. Recalling that reciprocal space is inverse to regular space, supercells with equal and large dimensions converge at smaller values of N, and inversly for cells of small dimsion. In supercells with different length axis, such as hexagonal cells, we use the notation $NxNxM$, where M relate to the distincntly different axis. The amount of kpoints required can be fruther reduced by utulizing the symmetry of the cell, in which we can exactly approximate the entire BZ by extending a lesser zone through symmertry. This reduced zone is appropriartly named the irreducible Brillouin zone (IBZ).

Metals in particular requiere a large set of kpoints to acchive accurate results. This is becouse we encounter discontinuies functions in the Brillouin zone around the fermi sufrace where the states discontinusly change from occupied to non-occupied. To reduce the cost of this operatin, there are two primary methods, tetrhaedon and smearing. The idea behind the tetrahedon method is to use the discrete set of k-points to fill the reciprocal space with tethraeda and interpolate the function within each tethraeda such that the function can be integrated in the entire space rather than at discrete points. The latter approach for solving discontinuos integrals is to smear out the discontinuity and thus transforming the integral to a continous one. A good analogy to this method is the fermi-dirac function, in which a small variable σ transform a step-functino into a continious function that can be integrated by standard methods.

In addition to the number of kpoints, there is one more distinct parameter that must be specified in DFT calculations, namely the energy cutoff, or E_{cut}. This parameters arise from the Bloch function described previosly. In which $u_{\boldsymbol{k}}(\boldsymbol{r})$ was a bloch wave with the same periodicity as the supercell. This implies that the wave can be expanded by a set of special plane waves as

$$u_{\boldsymbol{k}}(\boldsymbol{r}) = \sum_{\boldsymbol{G}} c_{\boldsymbol{G}} e^{i\boldsymbol{G}\boldsymbol{r}}, \tag{6.6}$$

where $\boldsymbol{G}$ is the reciprocal lattice vector. Combining this with eq ..(first eq for blcoh function) we get

$$\psi_{\boldsymbol{k}}(\boldsymbol{r}) = \sum_{\boldsymbol{G}} c_{\boldsymbol{k}+\boldsymbol{G}} e^{i(\boldsymbol{k}+\boldsymbol{G})\boldsymbol{r}} \tag{6.7}$$

The consequense from this expression is that evaluating the wavefunction of an electron at a single k point demand a summation over the entirity of reciprocal space. In order to reduce this computational burden, we can introduce a maximum paramater E_{cut} to cap the calculations. This is possible becouse eq ..(above) is the solution of the Shrödinger equation with kinetic energy

$$E = \frac{\hbar^2}{2m}|\boldsymbol{k}+\boldsymbol{G}|^2. \tag{6.8}$$

Seeing as the solution with lower energies are the most interesting, we can limit the calculations of eq ..(2 above) to solutions with energy less than E_{cut} given bellow

$$E_{\text{cut}} = \frac{\hbar^2}{2m} G_{\text{cut}}. \tag{6.9}$$

Thus, we can reduce the infinitly large sum above to a much more feasable calculation in

$$\psi_{\boldsymbol{k}}(\boldsymbol{r}) = \sum_{|\boldsymbol{k}+\boldsymbol{G}|<G_{\text{cut}}} c_{\boldsymbol{k}+\boldsymbol{G}} e^{i(\boldsymbol{k}+\boldsymbol{G})\boldsymbol{r}} \tag{6.10}$$

A summary on kpoints and ENCUT, plus a discussion on nummerical convergence and how to select kpoints and ENCUT

A final consideration to how DFT is applied in practise is how the core electrons are handled. Tightly bound core electrons as opposed to valene electrons demand a greater number of plane-waves to converge. The most efficient method of reducing the expenses of core-electrons are so-called pseudopotentials. This method works by approximating the electron density of the core elecrons by a constant density that mimic the properties of true ion core and core electrons. This density is then remained constant for all subsequent calculations, ie only considering the valence electrons while regarding the core electrons as frozen-in. There are currently two popular types of psudopotentials used in DFT, so-called ultrasoft psudopotentials (USPPs) devoplped by Vanderbilt, and the projecter augmented-wave (PAW) method by Bloch [10], [1].

6.3 Self-consistent field calculation

Needs work, see lecture notes ch 8, book ch1 Preceding this section, we have considered the fundamental theory of DFT and it's practical ability to model various materials. In figure 6.1 we present the self-consistent field calculation scheme for how DFT calculations are performed. The initial problem posed by dft is that all properties rely on the density, and are dependent on each other. For instance, the effective potential is dependent on the density, which again is dependent on the eigenfunctions, that rely on the effective potential again. The cleaver approach, as seen in figure 6.1 begin with an initial guess to the density from which we can solve the Kohn-Sham equation and obtain the corresponding eigenfunctions. Following is an iterative method where we apply the recently calculated eigenfunctions to determine a new density and repeat the procedure above. This is repeated until the total energy is converged, by an own-defined criterion. Equivalently, the optimal ionic positions can be found by a similar approach. This method is based on quasi-Newton algorithms to minimize the forces between ions.

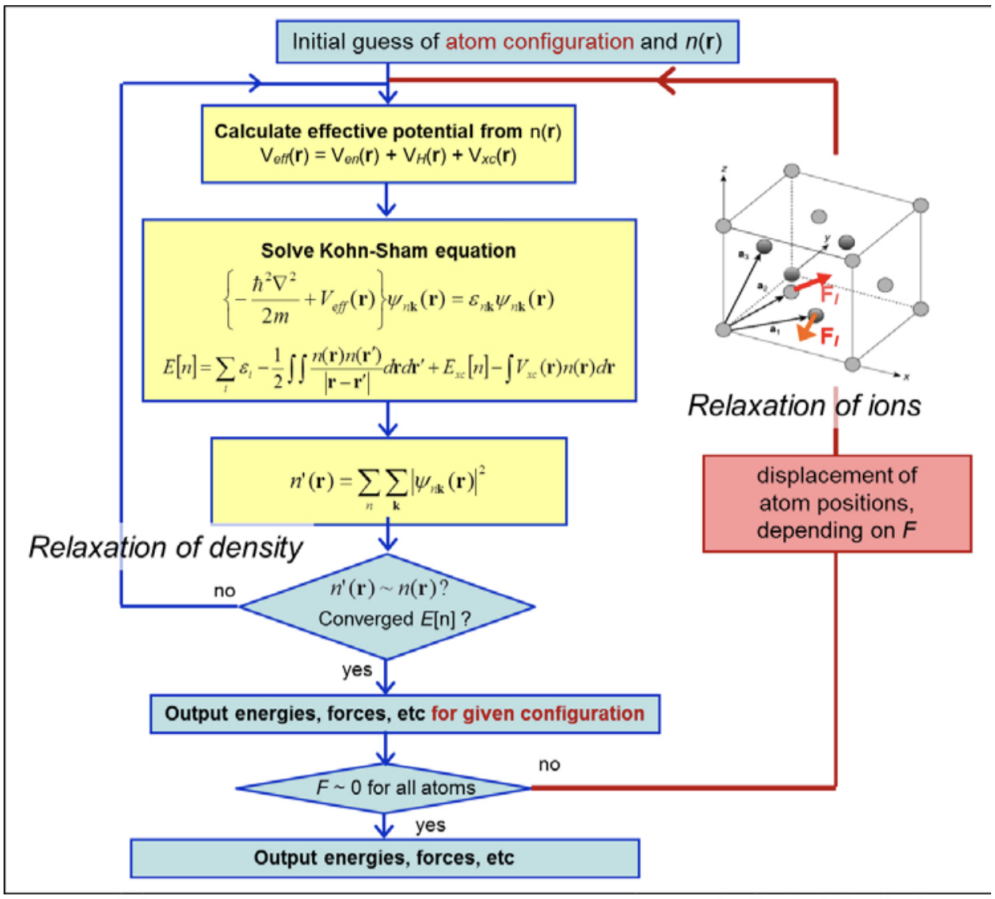

Figure 6.1: Self consistent iteration of a DFT calculation. Figure adopted from lecture notes fys-mena4111 **cite**

Chapter 7

Computational details

This section is intended to provide the necessary details for reproduction of results to be presented later on. First we begin by describing the software used for the project.

7.1 Vienna Ab initio Simulation Package

This software, often referred to as VASP is a package for ab initio quantum mechanics calculations using the projected augmented wave method and plane wave basis set. The intended methodology is DFT, but have been extended for methods post the original DFT-formulation. Calculations with VASP was carried out on the supercomputer fram, with allocated time and resources provided by Uninett Sigma2,**add reference!**.

The structure of VASP rely on a set of input files and output files from the calculation, the input files required to perform a DFT computation in VASP are the following:

- INCAR - this file provide the tags responsible for different methods, algorithms, parameters etc.
- POSCAR - this file is related to the crystal structure of the system
- POTCAR - What psudopotential that is used
- KPOINTS - A file containing information on what KPOINTS will be used
- jobfile - This file contains information for the supercomputer regarding resources and such.

The capitalization displayed above is directly related to the requirements of the file system in the VASP/fram collaboration. Some important output files are:

- CONTCAR - The relaxed crystal structure after finalized calculation
- CHGCAR - This file contains the electron density after calculation

- EIGENVAL - Contains the solutions to the Kohn-Sham eigenfunctions
- DOSCAR - Information on the Density of States
- OUTCAR - Contains a list of all other information.

Some figure or tables to make this information more presentable

In this project, we used the PAW psudopotential, and PBE GGA in favor of LDA for the reasons mentioned previously. Furthermore we readily employed meta-GGA functionals and hybrid-functionals, in particular SCAN and HSE06. We began the calculation of every individual structure by testing the convergence of total energy with respect to the number of k-points and cutoff energy. In VASP, the latter can be specified by setting the tag "ENCUT" in the INCAR file, we found 300 eV to yield productive results in terms of convergence and computation time for total energy calculations, and 400 for ionic+volume relaxations. Regarding the number of points in the reciprocal space, we carried out a great deal of simulations on numerous structures with distinct crystal structures and corresponding supercells, for this reason we employed a number of different sets of k-points depending on the structure. Typically the number of points ranged from a 2x2x2 mesh to 4x4x4 mesh. With the smaller being required for hybrid functionals to converge.

Upon realizing the convergence parameters, the structures were allowed to relax both the ionic positions, and cell volume with the quasi-newton method and a convergence criterion of $1E-2$ for the forces and $1E-5$ for the total energy. However, the symmetry of the structure was forced constant by the use of vasp-std-noshear. This process was repeated two times before performing final total energy calculation with various functionals.

The specific tags, algorithms, parameters and options of VASP that was in use throughout this project can be found at our GitHub address, but in particular we would like to cover two specific parameters. The First is related to the magnetic configuration of our calculations, specified with the tag ISPIN in VASP. We used ISPIN=2 which allow for co-linear spin-polarized calculations due to the involvement of ferromagnetic elements such as iron and nickel in this study. However, there are many more magnetic orientations the system can adopt besides co-linear, therefore the final total energies we found may not be the true lowest energies. But given the allocated duration and resources of this project, this is a understood consequence. Secondly is the type of smearing that was used for the different calculations. The preferred method for accurate total energies and density of states in semiconductors is the tetrahedron method [2], and for accurate forces in metals the Methfessel-Paxton method is recommended. However, our system contains both metals and a large portion of Si. For this reason we used a combination of smearing methods. For the relaxation and minimization of forces, we used gaussian smearing with smearing width $\sigma = 0.05$, as this method provide accurate forces in both metallic and semiconducting materials. And to calculate the total energy and

DOS, we used the tetrahedron method, as recommended. In order to obtain converged results of the HSE06 functional, we first calculated the charge density with gaussian smearing, then apply this density to perform a second hybrid calculation with the tetrahedron method. This was necessary becouse gaussion smearing yielded inaccurate and unreliable results in terms of the density of states when comparing to the band gap from the koh-Sham eigenvalues. However, this method, in addition to the narrow k-grid of just 2x2x2 k-points does include a factor of uncertainty regarding these results from the HSE06 functional.

This [4] is a good reference for extracting the band gap of VASP jobs relating to smearing and DOSCAR vs EIGENVAL

Band structure/DOS and band-unfolding?

7.2 Generation of SQS

Needs work, add part on filling ratio of ideal cube The generation of special quasi-random structures as described in section .., was done by utilizing the Temperature Dependent Effective Potential (TDEP) method. This package, devolved by Olle Hellman, offers a wide range of tools primary intended for studies of finite temperature lattice dynamics. In this project we utilize the program generate-structure within the TDEP package to construct SQS's. The work of TDEP is the result of an unpublished PHD thesis by Nina Shulumba **(Insert citation)**, thus the documentation on the software and generate-structure script is limited, please refer to the original author for more information.

In this project, we constructed SQS's by first transforming the cif-files of a given initial structure, for instance that of $FeSi_2$, to a primitive unit cell. The SQS's was generated by the same principles explained in section .., for each structure we created 5 distinct SQS's of an equal size under the constraint that the 3d atoms be distributed eqvimolar in the system. Precise file formats and such can be found at GitHub. Another approach could have been to construct SQS's of specific cell counts instead of total number of atoms, however this quickly lead to extremely large supercells, up to 256 atoms, that simply would not converge to our best efforts.

We began by studying high-entropy silicides by alloying 3d-metal silicides such as Fe_2Si by Cr, Fe, Co, and Ni to construct a $(CoCrFeNi)_2Si$ alloys. From this point we varied the distribution and type of elements in an attempt to locate high-entropy silicides with semiconducting properties, but remained within quaternary 3d silicides. Examples of SQSs generated by TDEP, from $FeSi_2$ structure with Cr, Fe, Mn and Ni can be seen in figure 7.1.

7.3 Band-structure

This [19] is an excellent reference for how one might calculate the band structure, use in this section, and include figures from text.

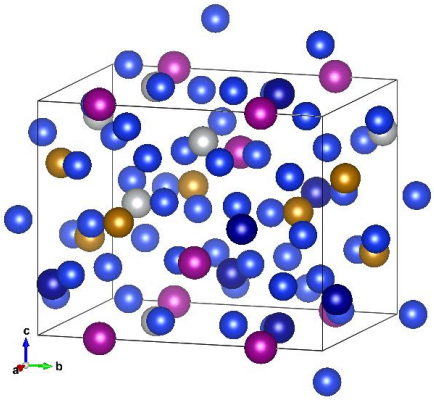

(a) Structure A

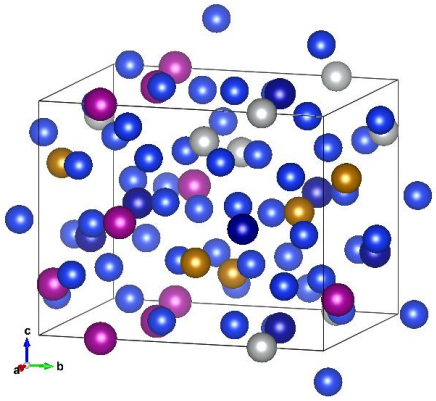

(b) Structure B

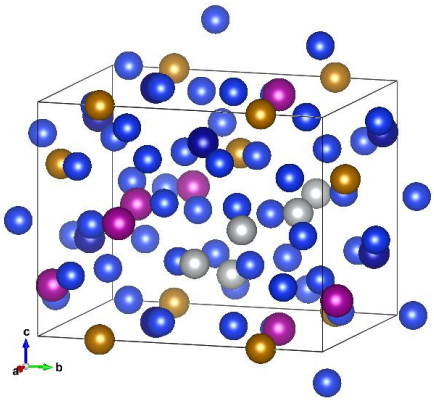

(c) Structure C

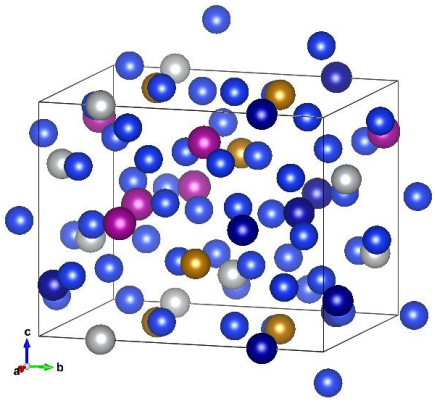

(d) Structure D

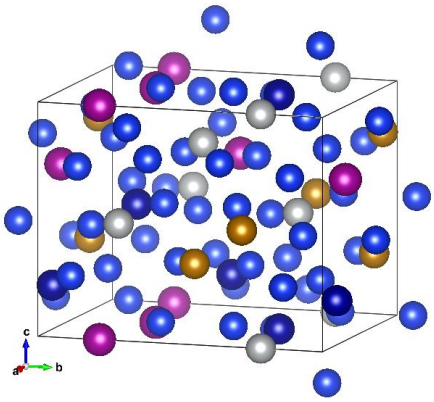

(e) Structure E

Figure 7.1: 48 atom SQS based on eqvimolar distribution of Cr, Fe, Mn and Ni in and $FeSi_2$ cell.

7.4 Utility scripts

During the course of the projects lifetime, several shell and python scripts was developed by myself and/or provided to me by my supervisor Ole Martin Løvvik and his team of researchers at Sintef. These can be located at the GitHub address :...

mm

Part III

Results and Discussion

Chapter 8

Working title

In the introduction to this project, we briefly discussed the scope and focus of the thesis. In figure/table .. we have displayed the complete list of structures, compositions and permutations of high-entropy silicides trialed throughout the duration of the project. **Make figure.** Amidst the large number of structures, we found particularly promising attributes of $(CrFeMnNi)Si_2$ (CFMN) SQSs based on the orthorombic crystal structure of $FeSi_2$, thus we will begin this section by presenting the results regarding this structure.

In this structure, each supercell consist of 48 total atoms, 32 of which is silicon, and the remaining 16 positions is equally distributed between Chromium, iron, manganese, and Nickel. The 5 distinct SQS supercells can be seen in figure (method/SQS). In table **??** we present a summary of the most relevant functional properties of the SQSs.

Structure	Total energy/atom (eV)	Final magnetic moment (?)	Band gap (eV)
A	-6,6080	4.0006	0.0280
B	-6,6138	3.9999	0.0523
C	-6,6063	4.0008	0.0344
D	-6,6155	4.0001	0
E	-6,6089	4.0000	0.0495

Table 8.1: Total energy per atom, final magnetic moment, and band gap (GGA) of 5 $Cr_4Fe_4Mn_4Ni_4Si_{32}$ SQSs based on $FeSi_2$

Bellow we have plotted the total density of states corresponding to the five distinct SQSs.

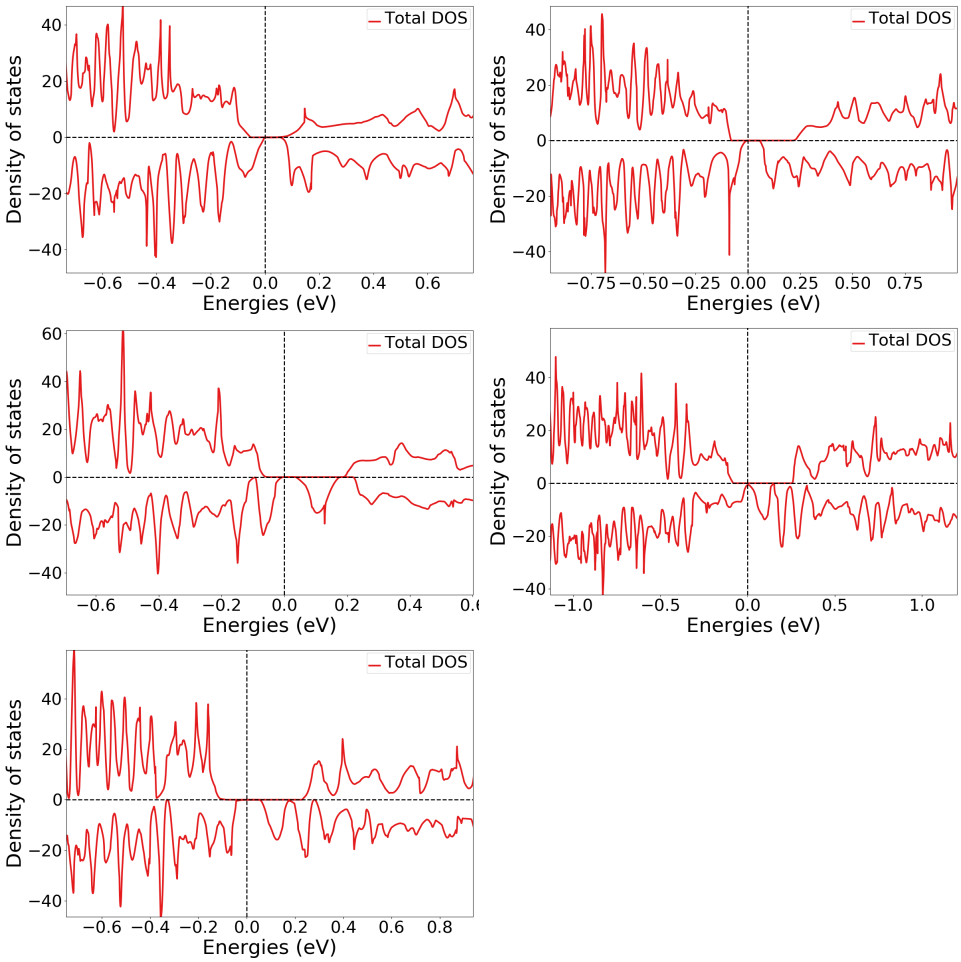

Figure 8.1: Density of states for structure A, B, C, D, E of $CFMNSi_2(FeSi_2)$ SQSs (PBE GGA)

Structure	Spin-up	Spin-down	Total
A	0.0814	0.0522	0.0281
B	0.2932	0.0523	0.0523
C	0.2355	0.0343	0.0343
D	0.3386	0	0
E	0.3078	0.0495	0.0495

Table 8.2: Band gap (GGA) in spin up and spin down channels of CFMNSi2 structures

Structure	PBE	SCAN	HSE06
A	0.0281	0.0000	0.0207
B	0.0523	0.0890	0.1808
C	0.0344	0.0690	0.0196
D	0.0000	0.0000	0.0000
E	0.0495	0.1048	0.0133

Table 8.3: Band gap of $CFMN(FeSi_2)$ SQSs with GGA (PBE), meta-GGA (SCAN) and hybrid-functionals (HSE06). **Add footnote to explain the uncertainty in these results regarding smearing type and width, and DOS and EIGENVAL**

Looking at the results from different functionals, we observe that the hybrid functional HSE06 more or less agree with results of the PBE functional in terms of the actual presence of the band gap, while the size of the gap is up for debate. Especially in B, where we observe a band gap greater than 0.18 eV in comparison to 0.05 eV with PBE and 0.08 with SCAN. Bellow we show the total density of states around the fermi energi E_f for this structure with the HSE06 functional.

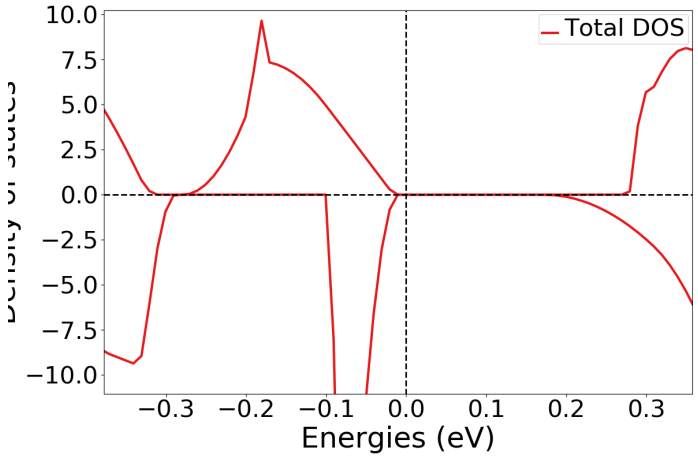

Figure 8.2: Density of states from HSE06 of $FeSi_2$ CFMN structure B

If we now compare this to the density of states of structure E,

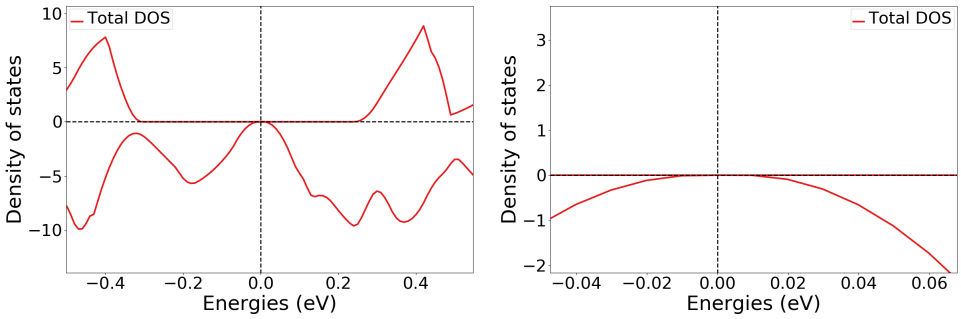

(a) DOS ↑, ↓ (b) DOS ↓

Figure 8.3: The density of states of CFMN ($FeSi_2$) structure E for a) spin up and down, and b) focused on spin down

it's obvious that the wider band gap of structure B stems from the spin down channel, as opposed to the other structure where we observe large gaps in ↑ and small nonzero gaps in ↓ except for D with metallic characteristic in spin ↓, responsible for the zero band gap displayed in table ..

I think its relevant and interesting to in-depth analyze structure B, D, and E. B because of large band gap. D because no band gap, and E because this well represents the other structures A and C. One difference is the KS eigenvalues. Str D have both partial occupancy and nonphysical occupancy, ie above 1 and bellow zero both in PBE and HSE06. This is not the case for structures that exhibited band gaps. Here we have clear transition from 1 to 0. Without having done a broad investigation of all material. This seems to be the case in other compositions and cells and permutations as well. Where both partial occupants and nonphysical occupations result in metallic structures. Calculating the band gap with strict 1 and 0 conditions, lead to small band gaps in most structures. Furthermore, in structures of Fe2Si, the difference in band where occupation transition from 1 to 0 between up and down, increases hugely compared to FeSi2 structures, talking close to 20 bands, opposed to maybe 2-5.

Part IV

Conclusion

Bibliography

[1] P. E. Blöchl. 'Projector augmented-wave method'. In: *Phys. Rev. B* 50 (24 Dec. 1994), pp. 17953–17979. DOI: 10.1103/PhysRevB.50.17953. URL: https://link.aps.org/doi/10.1103/PhysRevB.50.17953.

[2] Peter E. Blöchl, O. Jepsen and O. K. Andersen. 'Improved tetrahedron method for Brillouin-zone integrations'. In: *Phys. Rev. B* 49 (23 June 1994), pp. 16223–16233. DOI: 10.1103/PhysRevB.49.16223. URL: https://link.aps.org/doi/10.1103/PhysRevB.49.16223.

[3] Pedro Borlido et al. 'Large-Scale Benchmark of Exchange–Correlation Functionals for the Determination of Electronic Band Gaps of Solids'. In: *Journal of Chemical Theory and Computation* 15.9 (2019). PMID: 31306006, pp. 5069–5079. DOI: 10.1021/acs.jctc.9b00322. eprint: https://doi.org/10.1021/acs.jctc.9b00322. URL: https://doi.org/10.1021/acs.jctc.9b00322.

[4] Jürgen Furthmüller. *How might I calculate the exact bandgap from DOSCAR ?* May 2015.

[5] Michael C. Gao et al. 'Applications of Special Quasi-random Structures to High-Entropy Alloys'. In: *High-Entropy Alloys: Fundamentals and Applications*. Ed. by Michael C. Gao et al. Cham: Springer International Publishing, 2016, pp. 333–368. ISBN: 978-3-319-27013-5. DOI: 10.1007/978-3-319-27013-5_10. URL: https://doi.org/10.1007/978-3-319-27013-5_10.

[6] Alejandro Garza and Gustavo Scuseria. 'Predicting Band Gaps with Hybrid Density Functionals'. In: *The Journal of Physical Chemistry Letters* 7 (Aug. 2016). DOI: 10.1021/acs.jpclett.6b01807.

[7] Philip Hasnip. *Underestimation of Band gap by DFT?* Mar. 2016.

[8] Jochen Heyd, Gustavo E Scuseria and Matthias Ernzerhof. 'Hybrid functionals based on a screened Coulomb potential'. In: *The Journal of chemical physics* 118.18 (2003), pp. 8207–8215.

[9] Benjamin G. Janesko, Thomas M. Henderson and Gustavo E. Scuseria. 'Screened hybrid density functionals for solid-state chemistry and physics'. In: *Phys. Chem. Chem. Phys.* 11 (3 2009), pp. 443–454. DOI: 10.1039/B812838C. URL: http://dx.doi.org/10.1039/B812838C.

[10] G. Kresse and D. Joubert. 'From ultrasoft pseudopotentials to the projector augmented-wave method'. In: *Phys. Rev. B* 59 (3 Jan. 1999), pp. 1758–1775. DOI: 10.1103/PhysRevB.59.1758. URL: https://link.aps.org/doi/10.1103/PhysRevB.59.1758.

[11] Aliaksandr V. Krukau et al. 'Influence of the exchange screening parameter on the performance of screened hybrid functionals'. In: *The Journal of Chemical Physics* 125.22 (2006), p. 224106. DOI: 10.1063/1.2404663. eprint: https://doi.org/10.1063/1.2404663. URL: https://doi.org/10.1063/1.2404663.

[12] Z. W. Lu, S.-H. Wei and Alex Zunger. 'Electronic structure of ordered and disordered Cu_3 Au and Cu_3 Pd'. In: *Phys. Rev. B* 45 (18 May 1992), pp. 10314–10330. DOI: 10.1103/PhysRevB.45.10314. URL: https://link.aps.org/doi/10.1103/PhysRevB.45.10314.

[13] Lewis Robert Owen and Nicholas Gwilym Jones. 'Lattice distortions in high-entropy alloys'. In: *Journal of Materials Research* 33.19 (2018), pp. 2954–2969. DOI: 10.1557/jmr.2018.322.

[14] John P Perdew, Kieron Burke and Matthias Ernzerhof. 'Generalized gradient approximation made simple'. In: *Physical review letters* 77.18 (1996), p. 3865.

[15] John P Perdew and Yue Wang. 'Accurate and simple analytic representation of the electron-gas correlation energy'. In: *Physical review B* 45.23 (1992), p. 13244.

[16] John P. Perdew and Mel Levy. 'Physical Content of the Exact Kohn-Sham Orbital Energies: Band Gaps and Derivative Discontinuities'. In: *Phys. Rev. Lett.* 51 (20 Nov. 1983), pp. 1884–1887. DOI: 10.1103/PhysRevLett.51.1884. URL: https://link.aps.org/doi/10.1103/PhysRevLett.51.1884.

[17] John P. Perdew et al. 'Understanding band gaps of solids in generalized Kohn–Sham theory'. In: *Proceedings of the National Academy of Sciences* 114.11 (2017), pp. 2801–2806. DOI: 10.1073/pnas.1621352114. eprint: https://www.pnas.org/doi/pdf/10.1073/pnas.1621352114. URL: https://www.pnas.org/doi/abs/10.1073/pnas.1621352114.

[18] Muhammad Rashid et al. 'Ab-initio study of fundamental properties of ternary ZnO1-xSx alloys by using special quasi-random structures'. In: *Computational Materials Science* 91 (2014), pp. 285–291. ISSN: 0927-0256. DOI: https://doi.org/10.1016/j.commatsci.2014.04.032. URL: https://www.sciencedirect.com/science/article/pii/S0927025614002742.

[19] Wahyu Setyawan and Stefano Curtarolo. 'High-throughput electronic band structure calculations: Challenges and tools'. In: *Computational Materials Science* 49.2 (2010), pp. 299–312. ISSN: 0927-0256. DOI: https://doi.org/10.1016/j.commatsci.2010.05.010. URL: https://www.sciencedirect.com/science/article/pii/S0927025610002697.

[20] V. Sorkin et al. 'First-principles-based high-throughput computation for high entropy alloys with short range order'. In: *Journal of Alloys and Compounds* 882 (2021), p. 160776. ISSN: 0925-8388. DOI: https://doi.org/10.1016/j.jallcom.2021.160776. URL: https://www.sciencedirect.com/science/article/pii/S092583882102185X.

[21] Jianwei Sun, Adrienn Ruzsinszky and John P. Perdew. 'Strongly Constrained and Appropriately Normed Semilocal Density Functional'. In: *Phys. Rev. Lett.* 115 (3 July 2015), p. 036402. DOI: 10.1103/PhysRevLett.115.036402. URL: https://link.aps.org/doi/10.1103/PhysRevLett.115.036402.

[22] Jianwei Sun et al. 'Accurate first-principles structures and energies of diversely bonded systems from an efficient density functional'. In: *Nature chemistry* 8.9 (2016), pp. 831–836.

[23] Fuyang Tian. 'A Review of Solid-Solution Models of High-Entropy Alloys Based on Ab Initio Calculations'. In: *Frontiers in Materials* 4 (2017). ISSN: 2296-8016. DOI: 10.3389/fmats.2017.00036. URL: https://www.frontiersin.org/article/10.3389/fmats.2017.00036.

[24] Fabien Tran and Peter Blaha. 'Accurate Band Gaps of Semiconductors and Insulators with a Semilocal Exchange-Correlation Potential'. In: *Phys. Rev. Lett.* 102 (22 June 2009), p. 226401. DOI: 10.1103/PhysRevLett.102.226401. URL: https://link.aps.org/doi/10.1103/PhysRevLett.102.226401.

[25] Shen Wang et al. 'Comparison of two calculation models for high entropy alloys: Virtual crystal approximation and special quasi-random structure'. In: *Materials Letters* 282 (2021), p. 128754. ISSN: 0167-577X. DOI: https://doi.org/10.1016/j.matlet.2020.128754. URL: https://www.sciencedirect.com/science/article/pii/S0167577X20314610.

[26] Su-Huai Wei and Alex Zunger. 'Band offsets and optical bowings of chalcopyrites and Zn-based II-VI alloys'. In: *Journal of Applied Physics* 78.6 (1995), pp. 3846–3856. DOI: 10.1063/1.359901. eprint: https://doi.org/10.1063/1.359901. URL: https://doi.org/10.1063/1.359901.

[27] Peng Wei et al. 'Understanding magnetic behaviors of FeCoNiSi0.2M0.2 (M=Cr, Mn) high entropy alloys via first-principle calculation'. In: *Journal of Magnetism and Magnetic Materials* 519 (2021), p. 167432. ISSN: 0304-8853. DOI: https://doi.org/10.1016/j.jmmm.2020.167432. URL: https://www.sciencedirect.com/science/article/pii/S0304885320323994.

[28] S.-H. Wei et al. 'Electronic properties of random alloys: Special quasirandom structures'. In: *Phys. Rev. B* 42 (15 Nov. 1990), pp. 9622–9649. DOI: 10.1103/PhysRevB.42.9622. URL: https://link.aps.org/doi/10.1103/PhysRevB.42.9622.

[29] Jien-Wei Yeh. 'Overview of High-Entropy Alloys'. In: *High-Entropy Alloys: Fundamentals and Applications*. Ed. by Michael C. Gao et al. Cham: Springer International Publishing, 2016, pp. 1–19. ISBN: 978-3-319-27013-5. DOI: 10.1007/978-3-319-27013-5_1. URL: https://doi.org/10.1007/978-3-319-27013-5_1.

[30] Jien-Wei Yeh. 'Physical Metallurgy'. In: *High-Entropy Alloys: Fundamentals and Applications*. Ed. by Michael C. Gao et al. Cham: Springer International Publishing, 2016, pp. 51–113. ISBN: 978-3-319-27013-5. DOI: 10.1007/978-3-319-27013-5_3. URL: https://doi.org/10.1007/978-3-319-27013-5_3.

[31] Jien-Wei Yeh et al. 'Functional Properties'. In: *High-Entropy Alloys: Fundamentals and Applications*. Ed. by Michael C. Gao et al. Cham: Springer International Publishing, 2016, pp. 237–265. ISBN: 978-3-319-27013-5. DOI: 10.1007/978-3-319-27013-5_7. URL: https://doi.org/10.1007/978-3-319-27013-5_7.

[32] Yong Zhang et al. 'Phase Formation Rules'. In: *High-Entropy Alloys: Fundamentals and Applications*. Ed. by Michael C. Gao et al. Cham: Springer International Publishing, 2016, pp. 21–49. ISBN: 978-3-319-27013-5. DOI: 10.1007/978-3-319-27013-5_2. URL: https://doi.org/10.1007/978-3-319-27013-5_2.